Characterization of Calcium Carbonate, Calcium Oxide, and Calcium Hydroxide as Starting Point to the Improvement of Lime for Their Use in Construction

Miguel Galván-Ruiz[1]; Juan Hernández[2]; Leticia Baños[3]; Joaquín Noriega-Montes[4]; and Mario E. Rodríguez-García[5]

Abstract: In this paper a complete characterization of lime cycle transitions is described. $CaCO_3$ was collected from a Mexican mine and was processed to obtain $Ca(OH)_2$ through CaO. When the calcium hydroxide interacted with the CO_2 in the air forming $CaCO_3$, the lime cycle was completed. Crystal structure and spectroscopy characterization was carried out to get the knowledge of lime cycle $CaCO_3 \rightarrow CaO \rightarrow Ca(OH)_2 \rightarrow CaCO_3$ deeply. The changes in the crystalline structures were described using X-ray diffraction by powder to accomplish phase identification. Scanning electron microscopy was done to examine the morphology, topology, crystal structure, and crystalline growth habit. Dynamic light scattering was used to determine the particle-size distribution of $Ca(OH)_2$. Fourier-transform infrared was done to identify molecules and atomic bonds. Finally, inductively coupled plasma-mass spectrometry was done to get quantitative analyses. These results are a contribution to the restoration and construction industry fields, as well as a starting point to new possible applications of lime in current engineering.

DOI: 10.1061/(ASCE)0899-1561(2009)21:11(694)

CE Database subject headings: Lime; Calcium carbonate; Construction materials; Limestone.

Introduction

Lime is a burned variety of limestone ($CaCO_3$), commonly known as quicklime (CaO), or hydrated lime [$Ca(OH)_2$]. Initially limestone is extracted, crushed, and sieved; then it is fed into a kiln for preheating and calcination at temperatures between 900–1,200°C, decomposing it into calcium oxide (CaO) and carbon dioxide (CO_2). The original $CaCO_3$ loses 44% of its weight during calcination; afterward, the material is cooled and crushed. That is followed by hydratation process during slaking with the addition of an adequate amount of water to satisfy the chemical water affinity, thereby transforming the oxide into hydroxide. During hydratation, an exothermic reaction is produced and the solid nearly doubles its volume. As a final stage, the carbonation process, where $Ca(OH)_2$ acquires CO_2 from the environment, closes the cycle, returning to the starting point (Galván-Ruiz et al. 2009). Raw materials may have pollutants, or these could be added due to the calcination of fossil fuels and addition of water during hydratation (Galván-Ruiz et al. 2007). Boynton (1980) remarked the importance of lime for construction which has been extensively documented. Even though lime mortars have been used for centuries by earlier civilizations in many of the greatest structures, the Romans were the first to use it as a construction material, developing manufacturing methods based on natural cement, and creating appropriate construction techniques (Delatte 2001). In the 18th century, Smeaton started a scientific knowledge of the hydraulic limes which later derived into cement technology. Since the 19th century, the appearance of ordinary Portland cement (OPC) produced significant decreases in the use of lime because OPC offers fast setting and greater strength (Hill et al. 1992). The numerous environmental benefits to be gained in returning to a wider range of use of lime in buildings and construction are considerable. Some of those well-known factors include: production requires lower temperatures using less energy than OPC with less greenhouse emissions, and tolerates some degree of movement in the masonry, as compared to the stronger mortar based on OPC, which only allows lesser movement. However, the deterioration is caused by salts from the alkalis contained in OPC, not in lime compounds. Lower thermal conductivity, higher impermeability, and better adhesion to the ordinary masonry mate-

[1]Associate Professor, División de investigación y Posgrado, Facultad de Ingeniería, Universidad Autónoma de Querétaro, Centro Universitario Cerro de las Campanas s/n 76010, Querétaro, Mexico. E-mail: mgr@uaq.mx

[2]Associate Professor, CETIS 105-SEP, carr. a Tlacote s/n, Querétaro, Qro. 76148, Mexico. E-mail: jnhdez22@gmail.com

[3]Associate Researcher, Instituto de Investigaciones en Materiales, Universidad Nacional Autónoma de México, Ciudad Universitaria, C.P. 04510, Mexico. E-mail: simin@servidor.unam.mx

[4]Associate Professor, División de Investigación y Posgrado, Facultad de Ingeniería, Universidad Autónoma de Querétaro, Centro Universitario Cerro de las Campanas s/n 76010, Querétaro, Mexico. E-mail: joaquin@uaq.mx

[5]Professor, Departamento de Nanotecnología, Centro de Física Aplicada y Tecnología Avanzada, Universidad Nacional Autónoma de México Campus Juriquilla, Querétaro, A. P. 1-1010, C.P. 76000, Mexico (corresponding author). E-mail: marioga@fata.unam.mx

Note. This manuscript was submitted on March 19, 2007; approved on April 21, 2009; published online on October 15, 2009. Discussion period open until April 1, 2010; separate discussions must be submitted for individual papers. This technical note is part of the ***Journal of Materials in Civil Engineering***, Vol. 21, No. 11, November 1, 2009. ©ASCE, ISSN 0899-1561/2009/11-694–698/$25.00.

rials are compared to OPC-based products. Water retention means that lime continues to absorb and hold water into its mass (Holmes and Wingate 2003). Furthermore, mortars are dynamic materials, they continue interacting with their environment after the hardening and carbonation processes. The structures of crystalline phases were studied through X-ray diffraction (XRD) and scanning electron microscopy (SEM) in order to obtain information related to the particles morphology. Complementary energy dispersive spectroscopy was done to ascertain a semiquantitative elemental analysis. Dynamic light scattering (DLS) was used to determine the $Ca(OH)_2$ particle-size distribution. Atomic absorption spectroscopy (AAS), ion chromatography, and inductively coupled plasma-mass spectrometry (ICP-MS) were applied to obtain a quantitative elemental analysis, and Fourier-transform infrared was used to single out the molecules bonds. This report presents the physicochemical and mineralogical transitions produced during the lime manufacturing process as a starting point to the improvement and return to appropriate uses of lime in the construction industry.

Experimental Setup

Sampling

Three different samples were studied and labeled as follows: SA1 corresponds to $CaCO_3$, SA2 to CaO, and SA3 to $Ca(OH)_2$. Sample SA1 was obtained by collecting three samples of approximately 250 g from 12 different positions of limestone bank and repeatedly quartered down mixing all parts until a representative sample was derived. Sample SA2 was obtained as representative quick lime (CaO) from the kiln. Finally, Sample SA3 was acquired from the $Ca(OH)_2$ warehouse. All these samples were kept in a vacuum to avoid chemical reactions.

Methods

X-Ray Diffraction

The XRD patterns of SA1, SA2, and SA3 were done on a diffractometer (Siemens D5000, Germany) operated at 35-kV accelerating voltage and 15-A current, using Cu K_α radiation wavelength of 1.540 6 Å. The measurements were made at room temperature at a range of 10–70°C on 2θ with a step size of 0.05°.

Scanning Electron Microscopy

The microstructure and morphology of SA1, SA2, and SA3 samples were done using a scanning electron microscope (Jeol JSM 5600, Japan) using secondary electrons. The microscope was operated at 20-kV accelerating voltage.

Dynamic Light Scattering

Particle-size distribution of Sample SA3 was determined using DLS (Brookhaven Instruments BI-APD, U.S.A.) with 632.8-nm red laser, 90° scattering angle, 25°C ambient temperature, and 5 μs step time. 0.02 g of Ca(OH)2 was mixed with 20 ml of distiller water and stirred by hand at room temperature for 5 min. The first measurement was made immediately after stirring, the second was done 15 min later, and the final one was taken 30 min after. This was done in order to differentiate the complete particle-size distribution.

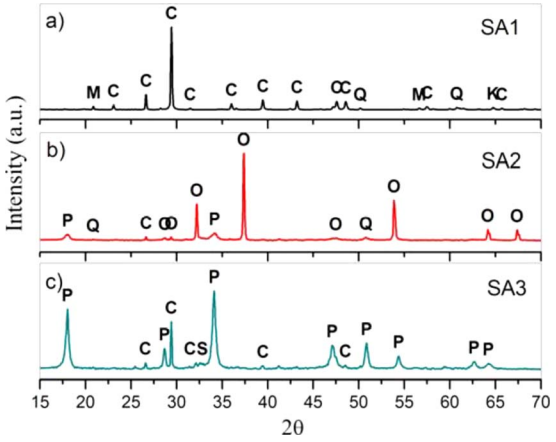

Fig. 1. XRD patterns of (a) SA1; (b) SA2; and (c) SA3; C-calcite, Q-quartz, M-muscovite, K-kaolinite, P-portlandite, O-calcium oxide, and S-calcium silicate

Inductively Coupled Plasma-Mass Spectrometry

Additional quantitative elemental analysis of the three samples was obtained by mass spectrometry (Thermo Elemental Mass system X-series ICP-MS, Standard Sample Introduction System, U.S.A.).

Fourier-transform infrared (FTIR) spectra were obtained by using spectrophotometer (Bruker vector 33, U.S.A.). The sample preparation consisted of mixing fine powders of each sample SA1, SA2, and SA3 with KBr powder. The specific technique used in the sample analysis was that of diffuse reflectance spectroscopy. The commercial samples were taken as references: $Ca(OH)_3$ (Baker analyzed 99.9%), CaO (Fermont 96.9%), and $Ca(OH)_2$ (Fermont 96.4%).

Results and Discussion

X-Ray Diffraction

The results of the analysis are presented in the outline of X-ray diffractograms used for phase identification. Fig. 1(a) shows the XRD pattern of SA1 samples produced from a hexagonal crystal structure corresponding to calcite ($CaCO_3$). These peaks were identified using Card No. 5-586 from International Center for Diffraction Data (ICDD) (see letter C). Other peaks from a hexagonal crystal structure corresponding to quartz (SiO_2) (Card No. 46-1045 ICDD) were identified as Q. The rest of the peaks are weaker signals corresponding to muscovite $[(KAl_2(Si_3Al)O_{10}(OH,F)_2)]$ (Card No. 07-0042 ICDD) (letter M), and kaolinite $[Al_2Si_2O_5(OH)_4)]$ (Card No. 06-0221 ICDD) (letter K). The lime was obtained from a mine where quartz is a common mineral component. Kaolinite and muscovite are also present components, but in a lower concentration. Fig. 1(b) shows the diffraction pattern of SA2. These pattern exhibit strong peaks corresponding to a face centered cubic crystal structure of CaO (letter O). Other peaks correspond to a hexagonal crystal structure from portlandite (Card No. 44-1481 ICDD) (letter P). The lower intensity peaks correspond to quartz and calcite. Here, quartz was

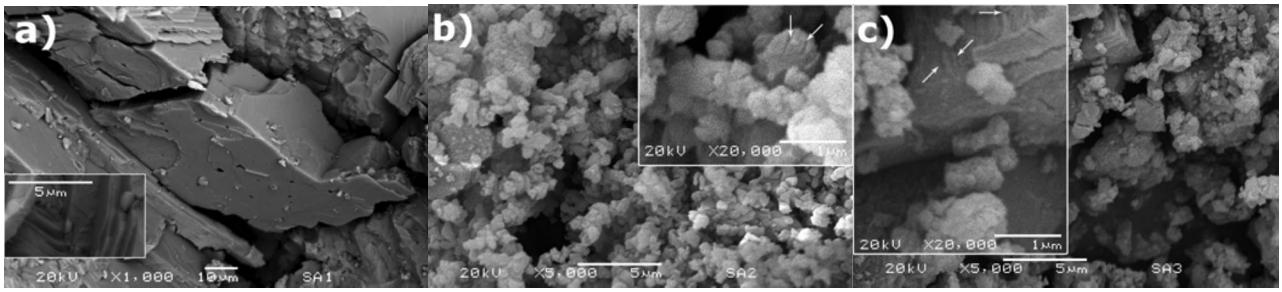

Fig. 2. SEM micrographs of (a) SA1; (b) SA2; and (c) SA3. In all images, the morphology of particles and the porosity of the different materials can be observed.

collected from the mine and remained unchanged during calcination process because quartz fusion temperature (2,000°C) is higher than that of calcite calcination. The presence of portlandite is due to the spontaneous reaction between CaO and moisture. Fig. 1(c) shows the XRD pattern of SA3. The strong peaks correspond to a hexagonal crystal structure of portlandite (P). In addition, weak peaks of calcite, quartz, and monoclinic crystals of calcium silicate (Card No. 86-0398 ICDD) (identified as CS) were also identified. Calcite in SA2 and SA3 is a remaining product from a low-efficiency transformation process to obtain CaO and $Ca(OH)_2$, respectively.

Scanning Electron Microscopy

Fig. 2(a) shows some rhombiclike blocks which have well-defined edges. Some ends are fragmented and reveal a layer structure (see the inset) which illustrates the crystal growth habit common to $CaCO_3$. The crystals also have pores and crevasses of varying length. The big size and well-defined shape of the crystals are a consequence of a good crystal growth process which requires a long time to take place. The crevasses could be the consequence of natural stress and/or sample preparation. Fig. 2(b) shows SA2 sample (CaO) which present amorphouslike particles. Their edges were not well defined and their shape is rounded. Furthermore, the inset exposes some relief lines on the particle surfaces (pointed with arrows). These lines may have originated during high temperature calcination reaction followed by a chilling process which produces a thermal shock in the material, creating these fissures on the surface. The material had many pores and continuous matrix appearance like it was made of attached particles. Their size distribution appears homogeneously dispersed around 800 nm.

In Fig. 3(c), most of the particles are smaller than 1 μm but the particle-size distribution is broad. Well-formed lumps observed in Fig. 3(c) were generated during dry-slaked lime process with water to transform nearly all of the CaO to $Ca(OH)_2$. On the other hand, calcium hydroxide reacts spontaneously with CO_2, forming $CaCO_3$ which is the most stable compound in the lime cycle. This is the reason why some particles with similar morphology were observed in Figs. 2(b and c). The inset in Fig. 2(c) presents a larger amplification of a particle with some surface lines (pointed with arrows) that were generated during crystal growth, thus revealing a preferential growth direction. The mechanical stress during the hydratation exothermal process produced cracks in the material volume. The crack propagation generated a submicron particle-size distribution, as it is described in the following DLS section.

Dynamic Light Scattering

Fig. 3 shows the particle-size distribution of SA3, in which three different measurements were done: one when immediately after the agitation process was completed [Fig. 3(a)], the second 15 min later [Fig. 3(b)], and the final one 30 min following the first measurement [Fig. 3(c)] (parallel structure). In the first measurement, major size particles were identified and the results were: 931.49 nm (41 counts), 853.10 (46), and 781.31 (44 counts). In the second measurement, particle-size distribution were: 327.48 nm (9 counts), 323.83 (47 counts), 320.22 (86 counts), 316.65 (100 counts), 313.12 (6 counts), and 309.63 (23 counts). Here it is possible to conclude that when the second measurement was made, the heavier particles had sunk to the bottom of the reservoir and lighter particles contributed to the size determination. Finally in the third measure, particle sizes were: 133.35 nm (48 counts), 100.00 (81 counts), 74.99 (100 counts), 56.23 (57 counts), and 42.17 (24 counts). In this last measure, particles lighter than those observed in the second measure contributed to the determination of the third particle size. The lime particle-size distribution is important because it influences some properties of stuccos and mortars such as adhesion, capillarity, porosity, and thermal and

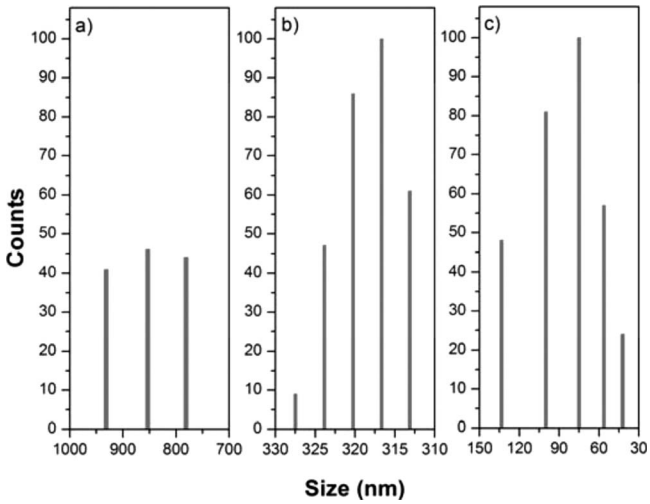

Fig. 3. Particles size distribution of SA3. Measures were done (a) immediately when dilution in bidistilled water was finished; (b) 15 min after first measure; and (c) 30 min after first measure.

Table 1. ICP-MS Analyses of SA1, SA2, and SA3

Sample	Li (mg/kg)	Be	V	Cr	Co	Ni	Cu	As	Se	Cd	Tl	Pb
SA1	1.3669	0.0	1.0211	0.0481	1.2674	2.3924	0.6621	0.4008	0.0	0.0	0.0536	0.8076
SA2	0.0087	0.0	1.9068	0.1066	0.0686	1.4785	0.2742	0.0290	0.0	0.0	0.0	0.0012
SA3	0.3401	0.0	4.3403	0.2150	0.0884	1.1589	0.1932	0.0849	0.0	0.0	0.0	0.0527

Note: Pb quantification can be done.

acoustic diffusivity. The particle-size distribution of lime is smaller than that in OPC. When CaO was hydrated, the energy generated for the spontaneous-exothermic reaction was done in a short time. The relatively short time of energy liberation caused the violent reaction and small portions of reacting material exploded producing $Ca(OH)_2$ with a submicron particle-size distribution.

Inductively Coupled Plasma-Mass Spectrometry

Table 1 summarizes the results of heavy metal content after ICP-MS analyses. Pb quantification was established exactly by this technique, contrasting with the result obtained through AAS, where the determination was noted just as under the quantification limit. The variation of vanadium content between SA2 and SA3 was relevant, with less content in SA1 before the addition of water to hydratation process.

Fourier Transform Infrared

The usefulness of qualitative analysis from the characteristic frequencies provides information to identify chemical constituents in a compound. Infrared spectra narrow the options to a few specific crystals if only one or two compounds are present. Additionally, a correlation of FTIR and XRD may be helpful. Fig. 4(a) shows the FTIR bands of SA1. The relatively low intensity band at 3,628 cm^{-1} corresponded to O–H bond matching with a low concentration of $Ca(OH)_2$ in the sample. The hydroxide is a remaining component of the carbonation process. The bands at 1,444, 877, and 713 cm^{-1} correspond to the three different elongation modes of C–O bonds while the bands at 2,980, 2,875, 2,513, and 794 cm^{-1} are harmonic vibration of these elongation modes. The width of this band implies that O–H groups must be forming hydrogen bridges. The minor bands at 2,875 cm^{-1} and the first overtone at 2,990 cm^{-1} correspond to C=O from carbonate ion. The thin and intense band at 1795 cm^{-1} is also associated to the carbonate C=O bonds. The very strong band at 1,444 cm^{-1} is related to the carbonate C–O bonds. The bands at 1,105, 1,018, and 790 cm^{-1} are related to SiO_2 (quartz), confirmed by the previous XRD analyses. The band at 713 cm^{-1} is related to Ca–O bonds. Comparing the spectra from a $CaCO_3$ standard (Baker analyzed 99.9%) with the SA1 spectra, the intense and sharp band at 877 cm^{-1} is assigned to $CaCO_3$ while the comparison between sample and standard spectra confirm very close similarity. Fig. 4(b) shows the spectrum of SA2 and comparison with standard of CaO spectrum. The strong band at 3,643 cm^{-1} corresponds to the O–H bonds from the remaining hydroxide (Park et al. 2002). The band at 1,417 cm^{-1} corresponds to C–O bond. The band centered at 866 cm^{-1} corresponds to C–O bond. The wide and strong band at around 500 cm^{-1} corresponds to the Ca–O bonds. This band is the largest one in the CaO standard spectrum but it is rather smaller in the SA2 spectrum.

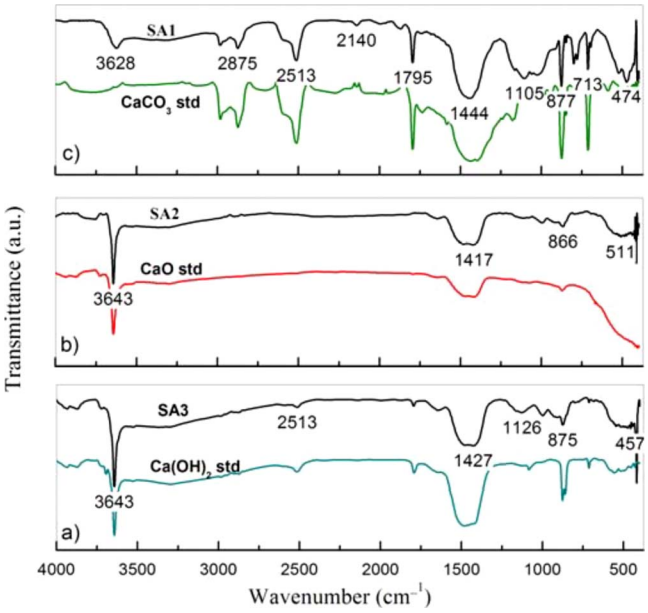

Fig. 4. FTIR spectra of (a) SA1 and $CaCO_3$ standard; (b) SA2 and CaO standard; and (c) SA3 and $Ca(OH)_2$ standard. Solid lines correspond to samples and dotted lines correspond to standards. In some bands, their corresponding vibrating groups are shown.

Fig. 4(c) shows the SA3 and $Ca(OH)_2$ standard spectra. The strong band at 3,643 cm^{-1} is related to the O–H bond from hydroxides. The band at 1,795 cm^{-1} corresponds to C=O bonds from carbonate. The intense and wide band at 1,427 cm^{-1} corresponds to C–O bonds from carbonate. The band at 875 cm^{-1} corresponds to Ca–O bonds. The weak band at 1,126 cm^{-1} corresponds to S–O bonds which reveals the presence of sulfur. This pollutant was possibly added by gases from the fuel oil combustion during the calcination process. The band in the region of 500 cm^{-1} corresponds to Ca=O bonds, possibly derived from the partial hydratation process. The $CaCO_3$ was collected from a Mexican mine and was transformed to CaO through a calcination reaction. This reaction had a low efficiency and consequently the CaO obtained had a considerable amount of $CaCO_3$ along with small amounts of the other minerals. These secondary minerals were not transformed either by the calcination reaction, or the subsequent reactions. Fuel combustion produced gases during calcination reaction, and this may generate sulfur contamination depending on the fuel quality. If a fuel rich in sulfurated organic compounds was used, the CaO produced would have more sulfur contamination. All the standard spectra closely matched with spectra samples, demonstrating that the process produces a loop cycle.

Conclusions

The aforementioned techniques offer a complete characterization of the lime cycle, and this information can be used for new applications where lime is used, such as construction, restoration, food additives, and others. It was possible to confirm how the different materials in each cycle stage were changing to form the most stable compound $CaCO_3$. This last stage is evidence that the lime cycle is dynamic and the transitions occur spontaneously. The process to produce $Ca(OH)_2$ from $CaCO_3$ has influenced in the morphological and topological features of lime particles. According to the XRD patterns, it was possible to identify each one of the crystalline phases of these materials. This is important in the industry because it allows the identification of any phase. In the construction industry, the XRD patterns allow the identification of these phases in mortars, stuccos, and plasters. The SEM images are a powerful tool to study the crystalline growth habits, and also the morphology and topology of the kinetic phases in lime cycles. The DLS for $Ca(OH)_2$ proved that the particle-size distribution is in the submicron range, indicative of lime can be used to reduce the porosity of compound materials used in the construction industry. The FTIR allows for the determination of specific bonds of molecules and to identify any phase of the lime cycle in compound materials. For restoration purposes, this technique is ideal because it allows for phase identification with a small sample resulting in a nondestructive sampling of historical buildings. The AAS and ICP are especially good techniques for a precise determination of chemical elements of contaminants for any stage of the lime cycle. It can also be used in the restoration to allow reformulation of the original materials used.

Acknowledgments

This work was developed with the generous collaboration of several people and organizations, technical support—Carolina Muñoz, Alicia del Real, Ofelia Pérez, Genoveva Hernandez—along with the support of CoSDAC-SEP (Project No. 022.09-P03), and FIFI-UAQ to whom we express our sincere gratefulness.

References

Boynton, R. S. (1980). *Chemistry and technology of lime and limestone*, Wiley, New York.

Delatte, N. J. (2001). "Lessons from Roman cement and concrete." *J. Profl. Issues Eng. Educ. Pract.*, 127(3), 109–115.

Galván-Ruiz, M., Baños, L., and Rodríguez-García, M. E. (2007). Lime characterization as a food additive." *Sens. & Instrumen. Food Qual.*, 1, 169–175.

Galván-Ruiz, M., Velázquez-Castillo, R., Pérez-Lara, M., Arjona, J. L., Baños, L., and Rodríguez-García, M. E. (2009). "Chemical and physical characterization of stuccos from a Mexican colonial building: 'El Museo del Calendario' of Querétaro." *Archaeometry*, Published Online: Feb. 2, 2009.

Hill, N., Holmes, S., and Mather, D. (1992). *Lime and other alternative cements*, Intermediate Technology Publications, U.K.

Holmes, S., and Wingate, M. (2003). *Building with lime*, ITDG Publishing, U.K.

Park, J., Min, D., and Song, H. (2002). "Structural investigation of CaO–Al2O3 and CaO–Al2O3–CaF2 slags via Fourier transform infrared spectra." *ISIJ Int.*, 42(1), 38–43.